Monolithic Bidirectional Power Transistors – Opening New Horizons in Power Electronics

J. Huber,
J. W. Kolar

Monolithic Bidirectional Power Transistors – Opening New Horizons in Power Electronics

Jonas Huber, *Senior Member, IEEE,* and Johann W. Kolar, *Fellow, IEEE*

I. INTRODUCTION

Today's global megatrends—loosely defined as long-term trends that shape societies and economies worldwide—include, e.g., the transition to a fully *renewable energy* supply and the establishment of evermore stringent efficiency requirements for industry. Similarly, the trend of *rapid global urbanization* creates a need for sustainable mobility. The *digital disruption* contributes to increased electricity demand but on the other hand enables solutions such as smart energy networks or design, control, and monitoring systems supported by artificial intelligence. Ultimately, thus, future energy systems should seamlessly integrate, e.g., renewable energy sources, electric mobility, and industrial plants, i.e., they will be mostly electric.

Power electronics is a key enabling technology for this transition to an all-electric society. Power electronic systems are and will be ubiquitous—be it as grid interfaces for datacenter power supplies (datacenters and data transmission networks consumed about 2% to 3% of the world's 2020 electricity production) or ultra-fast EV charging stations (the U.S. government targets a 50% EV market share by 2030), or as smart motor drives for industry automation (45% of all electricity powers electric motors, driving a wide variety of loads from pumps to highly dynamic actuators in robotics applications).

Both broad categories of power electronic converters, i.e., grid interfaces and motor drive systems, comprise widely used topologies that require switching elements with the capability of bipolar voltage blocking in the OFF state *and* bidirectional current conduction in the ON state, i.e., bidirectional switches (BDSs). **Fig. 1** shows two prominent examples: The Vienna rectifier (VR) [1] is a unidirectional three-phase, three-level ac-dc grid interface, widely used in telecom power supplies or EV chargers. The direct matrix converter (DMC) [2], [3] realizes ac-ac conversion for motor drives with only nine BDSs.
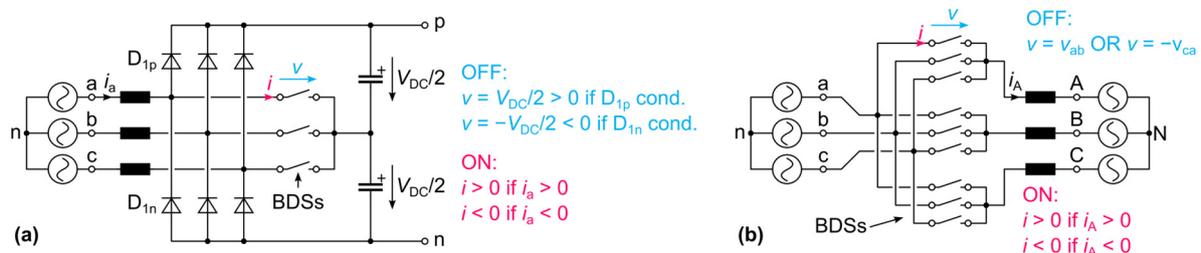

Fig. 1. Examples of converter topologies that require switching elements with bipolar voltage blocking and bidirectional current conduction capability, i.e., bidirectional switches (BDSs). **(a)** Vienna rectifier (VR) [1] a widely-used boost-type (note the grid-side boost inductors) topology for power-factor-correcting (PFC) rectifiers. **(b)** Direct matrix converter (DMC) [2], [3], an ac-ac motor drive topology with only nine BDSs.

However, none of the common power semiconductor devices (see **Fig. 2a-e**) provides the BDS functionality that these two—and many more—converter topologies require. Therefore, today's implementations must employ combinations of existing discrete devices. For example, an inverse-series connection of two MOSFETs achieves BDS functionality (see **Fig. 2f**), but the total on-state resistance increases to twice that of a single device. To prevent this, a second such inverse-series arrangement must be connected in parallel (see **Fig. 2g**). Thus, realizing BDS functionality with conventional power semiconductors, specifically with MOSFETs, comes at the price of a fourfold increase in chip area usage.

This factor-of-four penalty has, to some extent, hindered the two circuit topologies shown in **Fig. 1** from exploiting their full potential and might have slowed down the adoption of further topologies discussed throughout the article, which otherwise would offer significant advantages such as direct ac-ac conversion. With *monolithic* bidirectional switches (M-BDSs) and, in particular, M-BDSs with a single shared drift region for blocking either voltage polarity and two gates (one for controlling each blocking voltage polarity) as shown in **Fig. 2h** nearing market entry, a reevaluation of these converter

topologies becomes necessary. It is important to highlight that even though the common acronym M-BDS only includes the functionality (BDS) and the realization (M) but not the key aspect of having just a single drift region, in the following M-BDS refers to dual-gate single-drift-region devices like that shown in **Fig. 2h** (see also the specific example in **Fig. 15a**), unless stated otherwise. Focusing on the two key application areas of power electronics mentioned above (grid interfaces and motor drives), this article gives an overview on converter families that will benefit from M-BDSs and briefly discusses most recent M-BDS device concepts.
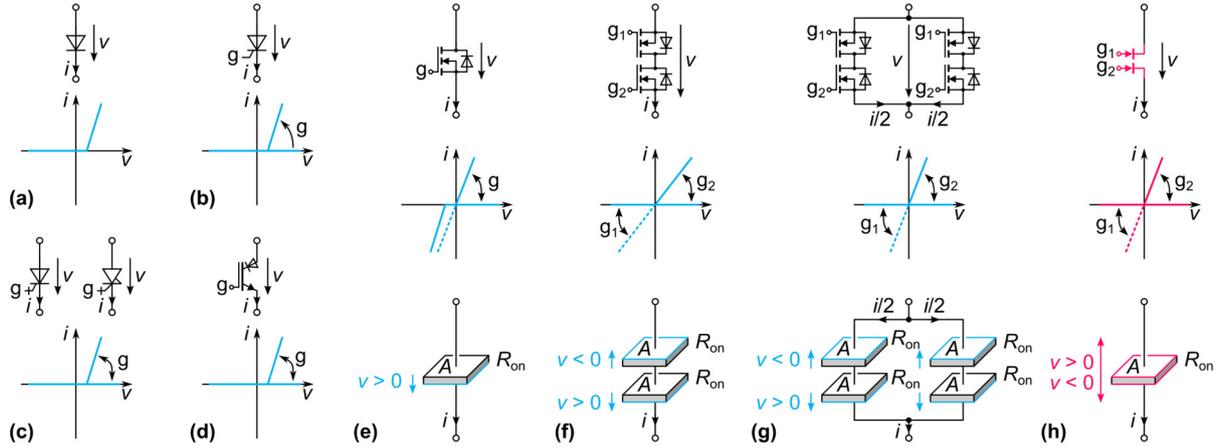

Fig. 2. Common power semiconductors and their *v-i* characteristics. **(a)** Diode. **(b)** Thyristors (without turn-off capability), **(c)** GTOs and IGCTs (with turn-off capability), and **(d)** RB-IGBTs (with reverse-blocking capability) can support both blocking voltage polarities but conduct only one current direction. **(e)** MOSFETs, in contrast, can conduct current in both directions but only support one polarity of the blocking voltage. For a given blocking voltage rating and a given chip area A, an on-state resistance of R_{on} results. **(f)** An inverse-series connection of two MOSFETs realizes BDS functionality but with a total resistance of $2\,R_{on}$; **(g)** paralleling a second such inverse-series arrangement again results in a total resistance of R_{on} but requires a chip area of $4\,A$, i.e., four times that of a single transistor. **(h)** Dual-gate single-drift-region monolithic bidirectional switch (M-BDS) with a single drift region used for blocking either voltage polarity, thus providing BDS functionality with a total on-state resistance R_{on} and only a minor increase of the chip area compared to a standard device without reverse-blocking capability.

II. THREE-PHASE GRID INTERFACES

Three-phase ac-dc grid interfaces are widely used in generic power supply applications (e.g., for telecommunication equipment, etc.) or, as shown in **Fig. 3**, for EV battery charging. Typically, galvanic isolation is realized with a dedicated isolated dc-dc converter stage (see **Fig. 3a**), or, alternatively, it might be integrated into the grid interface, which then realizes single-stage isolated ac-dc conversion as shown in **Fig. 3b**. In both cases, bidirectional power flow capability may or may not be required. Finally, dc-ac grid interfaces connect renewable energy sources such as PV to the mains (see **Fig. 3c**) and thus provide power flow from the dc to the ac side. Various converter topologies for such three-phase grid interfaces will strongly benefit from the availability of M-BDSs, as will be outlined in the following.
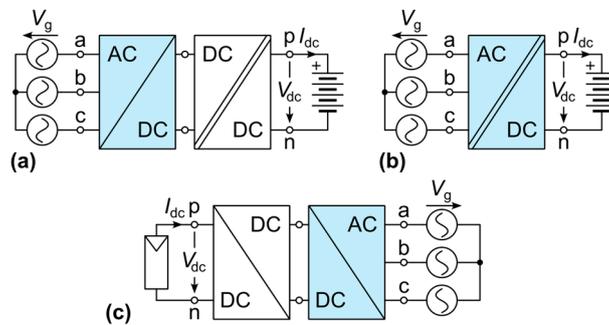

Fig. 3. Examples of three-phase grid interfaces. **(a)** Non-isolated ac-dc rectifier with a dc-dc isolation stage or **(b)** isolated single-stage ac-dc converter for EV battery charging. **(c)** Non-isolated dc-ac grid interface with opposite power flow direction for connecting a PV plant to the three-phase mains.

A. Third-Harmonic-Injection Rectifiers

The simplest way of realizing unidirectional ac-dc conversion is a passive diode rectifier. However, the resulting low-frequency mains current distortions are usually not acceptable. The integrated-active-filter (IAF) rectifier [4] shown in **Fig. 4a** extends the diode bridge by a high-frequency-(HF)-operated bridge-leg, an inductor, and three phase-selector BDSs operated at mains frequency, which allows to inject a third-harmonic current into the phase with the lowest voltage (absolute value) and hence achieve sinusoidal grid currents and power factor correction (PFC) functionality. The dc output voltage, however, is defined by the difference of the maximum and the minimum grid phase voltages and hence not controlled. Output voltage control could be achieved by connecting a buck converter stage, or, advantageously, by integration of that buck stage and the IAF's HF-operated bridge-leg, which results in the Swiss rectifier [5] shown in **Fig. 4b**. Whereas the Swiss rectifier is a buck-type ac-dc converter, i.e., the dc output voltage cannot exceed $V_{dc} \leq \sqrt{2/3}\, V_{g,ll}$ ($V_{g,ll}$ is the rms line-to-line grid voltage), a complementary, i.e., a boost-type ($V_{dc} \geq \sqrt{2}\, V_{g,ll}$) version can be realized [6], too, as shown in **Fig. 4c**.
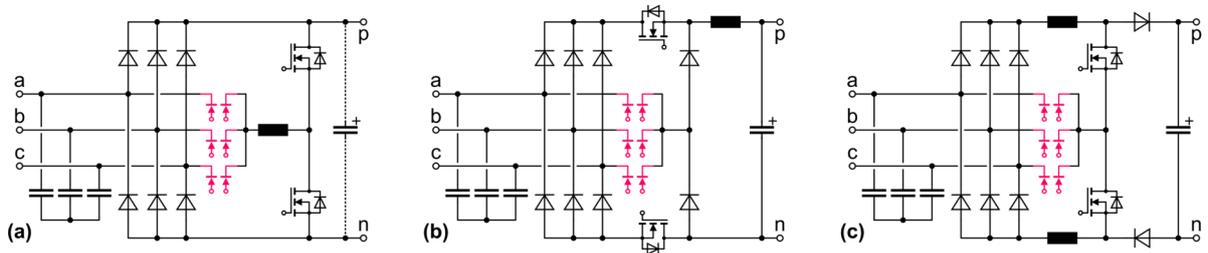

Fig. 4. Third-harmonic-injection rectifiers. **(a)** Integrated-active-filter (IAF) PFC rectifier without dc voltage control [4]. **(b)** Swiss rectifier [5] and **(c)** its boost-type variant [6].

B. Vienna Rectifier / T-Type Inverter

In the IAF rectifier, the grid voltage defines the conduction state of the diode bridge (i.e., it is line-commutated) and hence the dc output voltage. Shifting the IAF rectifier's inductor to the ac side (one per phase) decouples the diode bridge from the grid and hence allows to define its switching state using the phase-selector switches (i.e., it is forced-commutated) that are then directly connected to a capacitive DC-link midpoint. The resulting Vienna rectifier (VR) topology [1] mentioned above and shown in **Fig. 5a** thus achieves sinusoidal grid currents and a controlled dc output voltage using HF pulse-width modulation (PWM) of the phase-selector switches. The VR is a widely used boost-type PFC rectifier that advantageously features three-level bridge-legs (each switch-node can be connected to p, n or m, depending on the switching state and the phase current direction) and thus reduced grid-side filtering effort. Note that the M-BDSs need to block only half of the total dc output voltage, which, e.g., allows to use ±600 V GaN M-BDSs in a VR interfacing a 400 V grid to an 800 V dc output [7]. Alternatively, the delta-switch rectifier [8] shown in **Fig. 5b** does not require a dc-bus midpoint connection but stresses the M-BDSs with the full dc output voltage. Finally, the VR diodes can be replaced by transistors (rated for the full dc output voltage) to obtain the well-known T-type [7], [9] structure from **Fig. 5c**, which supports bidirectional power flow.

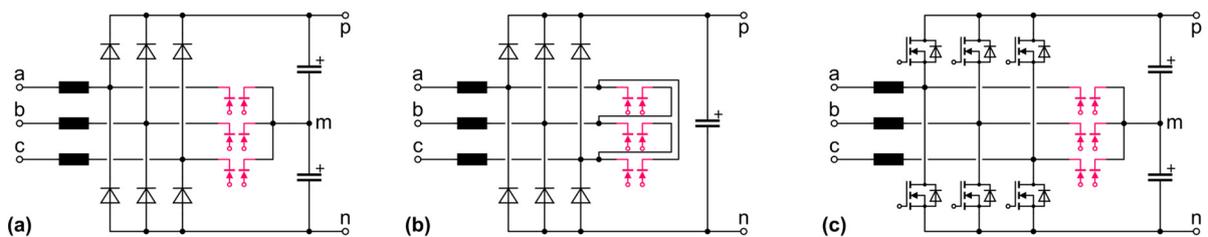**Fig. 5. (a)** Vienna rectifier (VR) [1]. **(b)** Delta-switch rectifier [8]. **(c)** Bidirectional three-level T-type rectifier/inverter [7], [9].

C. Three-Phase Buck-Boost PFC Rectifiers

Typical EV battery voltage ratings vary between 400 V and 800 V, and the actual battery voltage changes with the state of charge. Therefore, universal EV battery chargers must provide a wide dc output

voltage range, e.g., from 200 V to 1000 V as indicated in **Fig. 6a**. This wide output voltage range must typically be provided by the ac-dc grid interface (at least partly if an isolated dc-dc converter with a certain regulation capability is employed, fully in case of emerging non-isolated EV chargers), i.e., it must provide buck-boost functionality. A first option to achieve this is the combination of a boost-type PFC rectifier, specifically a (bidirectional) VR, and a buck-type three-level dc-dc stage as shown in **Fig. 6b**.

The VR is a voltage-source rectifier (VSR), i.e., it features a dc-link capacitor providing a constant voltage for the converter bridge-legs. Intuitively, it can be expected that a dual topology, i.e., a current-source rectifier (CSR) with a constant dc-link *current* exists, too. The duality relationship between the two topologies has been formally described on the switch and topology level [10], [11] and **Fig. 6c** shows, as an example, the duality between the MOSFET switching element used in VSRs and its dual, a series connection of a transistor and a diode providing bipolar voltage blocking but only unidirectional current conduction capability. A dual-gate M-BDS provides additional flexibility, especially bidirectional current conduction. This is required in the current-source-rectifier-(CSR)-based buck-boost topology [12] shown in **Fig. 6d** if bidirectional power flow should be supported and hence, due to the fixed polarity of the dc output voltage, both dc-link current directions are needed. Note that the main magnetic components (i.e., the dc-link inductor and the first-stage common-mode filter inductor) can be shared between the CSR and the dc-dc converter stage, facilitating improved power density and reduced implementation effort compared to the boost-buck VSR topology. On the other hand, the buck-boost CSR's M-BDSs must block the grid line-to-line voltage, i.e., ±900 V or ±1200 V devices are needed for 400 V grid applications (compared to the ±600 V rating of the VR's M-BDSs mentioned earlier).
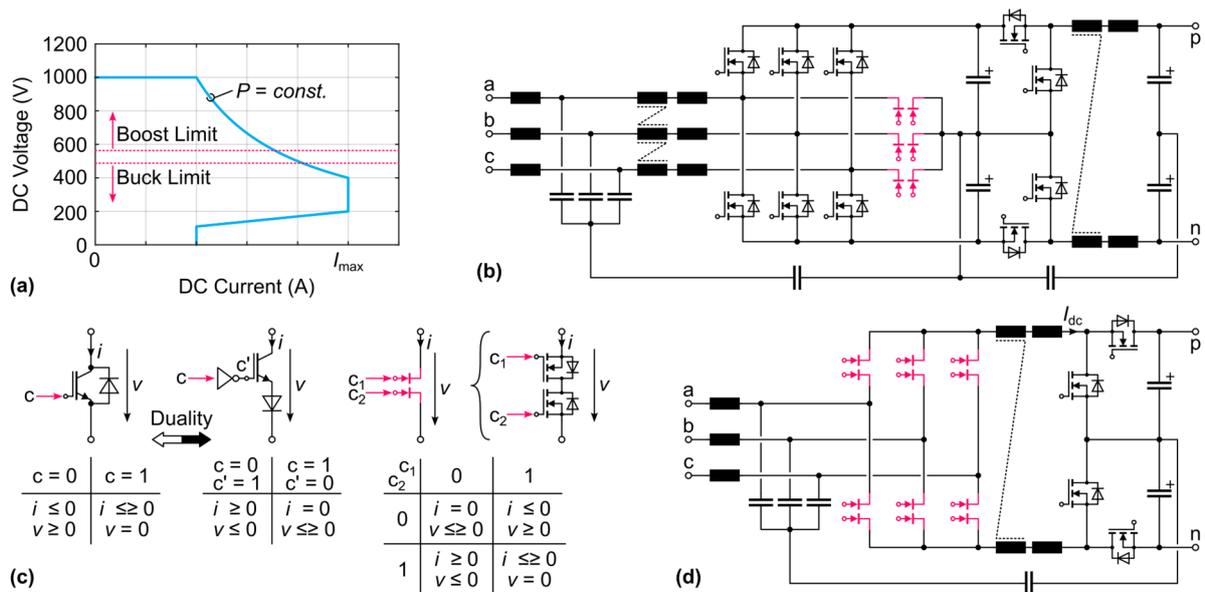

Fig. 6. (a) Output voltage/current operating range for general purpose EV charger modules, indicating the need for buck-boost functionality of the grid interface. **(b)** Voltage-source boost-buck rectifier based on a (boost-type) VR and a buck-type three-level dc-dc stage. **(c)** Duality relation [10], [11] between a switching device with unipolar blocking and bidirectional current conduction capability and one with bipolar voltage blocking but unidirectional current conduction capability; a dual-gate M-BDS can mimic both functionalities. **(d)** Current-source buck-boost rectifier topology [12], i.e., a buck-type current-source rectifier combined with a three-level boost-type dc-dc converter; note the advantageous sharing of the main magnetic components between the stages.

D. Isolated Three-Phase Grid Interfaces

The fully symmetric (if realized with M-BDSs) structure of the CSR stage discussed above opens the possibility of advantageously integrating galvanic isolation into the ac-dc stage (see also **Fig. 3b**), resulting in the isolated single-stage matrix-type ac-dc dual active bridge (DAB) converter [13], [14] shown in **Fig. 7a**. The CSR stage can synthesize an amplitude-modulated (six-pulse shape) primary-side HF transformer voltage from sections of the line-to-line voltages and employ the freewheeling state to compensate for that amplitude variation. Like a DAB, the CSR stage thus shapes the transformer current together with the secondary-side full-bridge to realize a desired (constant) power transfer while achieving optimization targets such as minimum rms current or soft-switching of the power semiconductors. Finally, the CSR stage's switching sequences ensure that in each switching period the

HF transformer current is distributed to all three input phases such that sinusoidal local average grid currents and thus a constant three-phase power flow result. Note that also variants of the VR with integrated galvanic isolation exist, e.g., the Vienna rectifier II [15] with unidirectional power flow capability as shown in **Fig. 7b**.
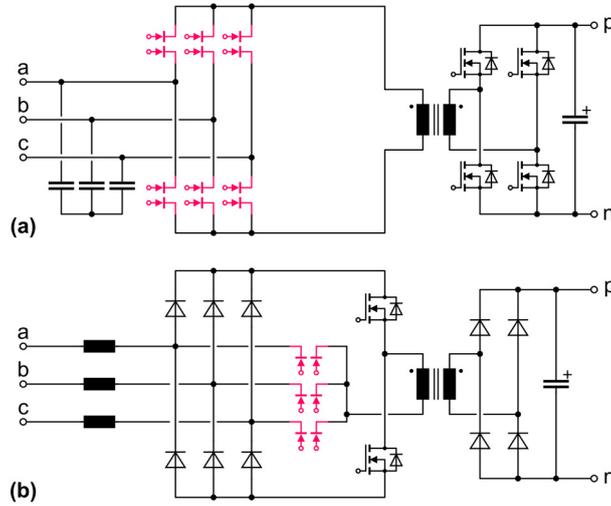

Fig. 7. (a) Bidirectional matrix-type ac-dc dual active bridge (DAB) converter [13], [14]. **(b)** Unidirectional Vienna rectifier II [15].

E. Single-Phase Grid Interfaces

Allow a brief digression from the article's focus on three-phase systems: there are, of course, also single-phase grid interfaces that benefit from M-BDSs. For example, the isolated matrix-type ac-dc DAB topology from **Fig. 7a** can also be realized with a single-phase ac interface [16]. Regarding single-phase PV microinverters, *non-isolated* topologies are of high interest due to high efficiency and comparably lower realization effort. However, suitable topologies should not generate a HF common-mode (CM) voltage at the dc output terminals, which would drive significant leakage currents through the PV panel's relatively large earth capacitance. The Highly Efficient and Reliable Inverter Concept (HERIC) [17] shown in **Fig. 8** uses an ac-side BDS switch, operated at the mains frequency, to realize the freewheeling states needed for the sinusoidal shaping of the grid current, which ultimately eliminates any HF CM voltage at the dc output terminals.
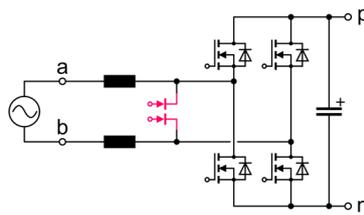

Fig. 8. Highly Efficient and Reliable Inverter Concept (HERIC) for single-phase non-isolated PV inverters [17].

III. MOTOR DRIVE SYSTEMS

Variable-speed drives (VSDs) are a second key application area of power electronics. As mentioned earlier, VSDs are used, e.g., to efficiently drive simple pump and blowers under varying load conditions, in electric vehicle traction chains, and in highly dynamic industry automation and robotics applications. Wide-bandgap (WBG) power semiconductors have the potential of significantly improving the efficiency of such motor drive systems, however, at the price of inherently steeper slopes of the switched voltages (higher *dv/dt*). Therefore, WBG-based VSDs must typically be equipped with output filters to achieve motor-friendly continuous output voltages (or at least *dv/dt*-limitation), which prevents issues such as reflections on long motor cables and resulting transient overvoltage isolation stresses, HF common-mode ground currents that degrade bearing lifetime, and it facilitates electromagnetic compatibility (EMC) without the need for expensive shielded motor cables. As WBG devices allow

much higher switching frequencies, the output filters can be comparably small. It has been demonstrated that the overall efficiency of a GaN-based drive system with LC output filter is higher than that of a conventional IGBT-based drive system without output filter [18], also due to the lower harmonic motor losses resulting from the GaN-based drive's smooth sinusoidal output voltages. Finally, there is a clear trend towards integrating VSDs directly with the motor [19] to simplify the interfaces and facilitate plug-and-play capability, i.e., high compactness and high efficiency due to typically constrained cooling possibilities in close proximity to the motor are further key features of future VSDs. **Fig. 9** gives a conceptual overview on typical motor drive configurations, i.e., dc-ac inverters, possibly with buck-boost functionality when operating from batteries or fuel cells, and grid-connected ac-ac VSDs. Again, for all cases with their partly differing requirements there are converter topologies that require BDSs and hence will significantly benefit from the availability of M-BDSs.
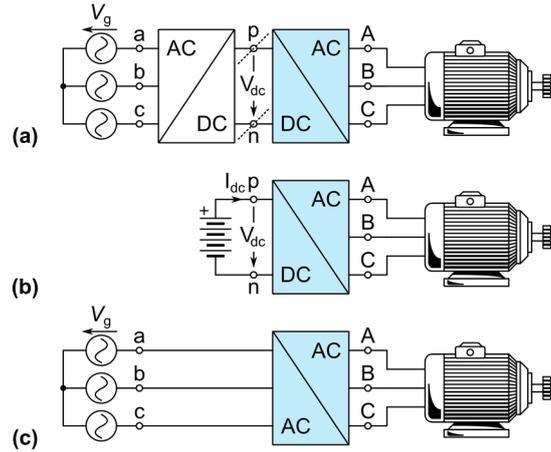

Fig. 9. Variable-speed drive (VSD) system concepts. **(a)** Motor inverter operating from a (shared) DC bus. **(b)** Operating from a battery (or a fuel cell) with a strongly load-dependent dc voltage requires a dc-ac inverter with buck-boost functionality. **(c)** Grid-connected ac-ac VSD.
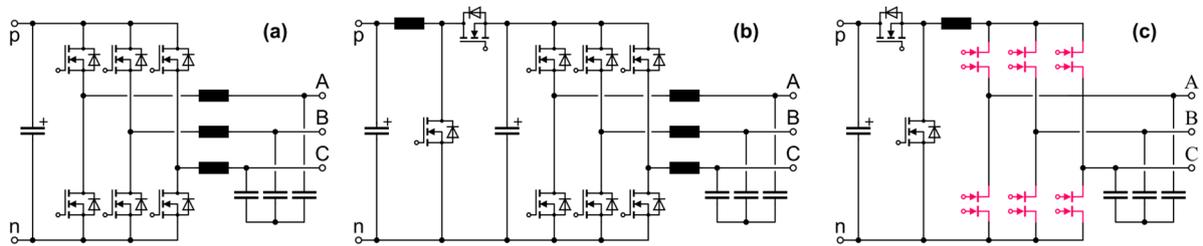

Fig. 10. Motor drive inverters operating from a (possibly shared) dc bus (see **Fig. 9ab**). **(a)** Voltage-source inverter (VSI) with LC output filter and thus sinusoidal motor voltages. **(b)** VSI with a dc-dc boost input stage to achieve boost-buck functionality. **(c)** Current-source inverter (CSI) with inherently sinusoidal output voltages and buck-boost functionality (note that the dc-dc buck stage is needed for voltage-to-current conversion).

A. DC-AC Motor Drive Inverters

Fig. 10a shows a voltage-source inverter (VSI) with an LC output filter to achieve smooth sinusoidal motor voltages. Note that the basic VSI topology is limited to buck operation, i.e., the peak motor line-to-line voltage cannot exceed the dc input voltage. However, if the VSD operates from a battery or a fuel cell, which show significant voltage variation depending on the state of charge or the load current, buck-boost functionality might be required to always provide sufficiently high output voltages for operating the motor over the full speed range. Thus, the VSI could be complemented by a dc-dc boost stage as shown in **Fig. 10b**. Note that three-level topologies, i.e., bidirectional versions of some of the rectifier topologies discussed above, could be employed, too, e.g., the T-type topology from **Fig. 5c** or, including the dc-dc stage, from **Fig. 6b**.

On the other hand, current-source inverters (CSIs) as shown in **Fig. 10c** require BDSs but inherently provide sinusoidal output voltages with only a single main magnetic component (the dc-link inductor) [19], [20]. Further, a dc-dc buck input stage is required to generate the dc-link current from the available dc input voltage (shared bus, battery, etc.), i.e., the topology inherently features buck-boost capability.

Note that the dc-dc stage can advantageously shape the dc-link current such that the CSI stages' switching losses are minimized by clamping one phase at all times (synergetic control of the two stages) [20].

B. AC-AC Motor Drives

Thyristor-based line-commutated inverters (LCI), see **Fig. 11a**, have been used in ac-ac motor drives since the 1970s and, typically in the megawatt power range, still are today. However, as the name implies, LCIs rely on externally defined ac voltages for the commutation of the thyristors, i.e., they only work with synchronous machines and the switching frequency is fixed by the grid/motor fundamental frequencies. Modern power semiconductors with turn-off capability facilitate current-source converters (CSCs, i.e., back-to-back connections of a CSR and a CSI with a shared dc-link inductor) with PWM operation of the rectifier and the inverter stages, resulting in advantages such as smaller dc-link inductors, higher control bandwidth, and improved harmonic performance [21]. However, note that unlike bidirectional CSRs, where the polarity of the dc-side voltage is fixed due to the dc output, ac-ac CSCs can process both power flow directions with the same, fixed dc-link current direction (note also the LCI's thyristors) by simply changing the polarity of the dc-side voltages of their CSR and CSI stages.
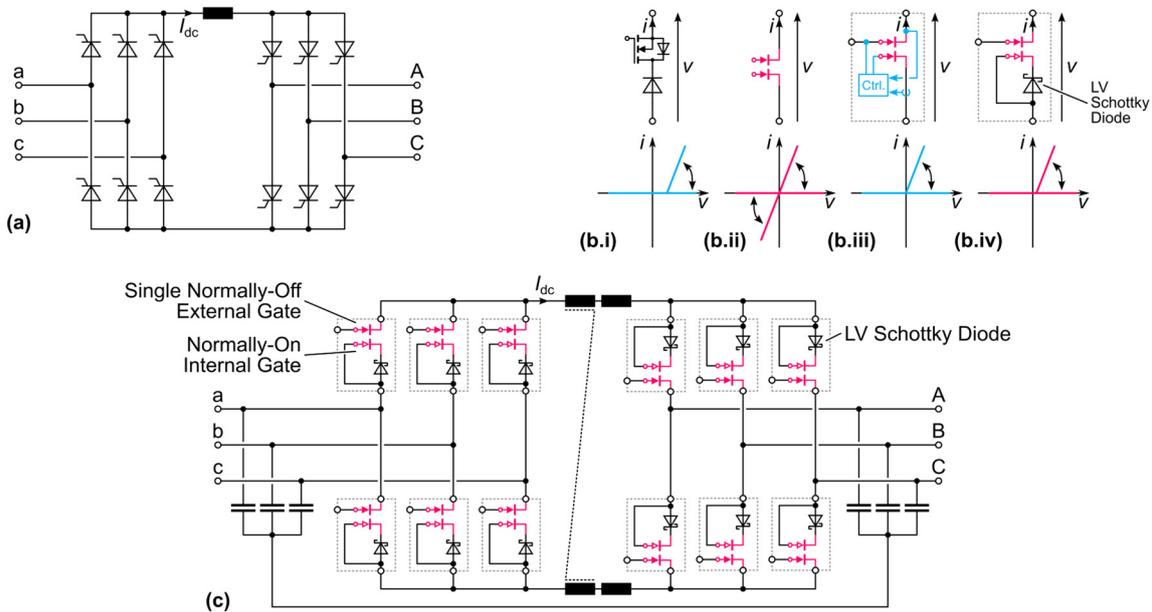

Fig. 11. (a) Motor drive based on line-commutated inverters (LCI). **(b)** Realization of the minimum required functionality (bipolar voltage blocking but only unidirectional current conduction) for ac-ac current-source converters (CSCs) without the drawback of **(b.i)** a high-voltage series diode by using **(b.ii)** M-BDSs and, to reduce complexity, **(b.iii)** advanced self-switching gate drives or **(b.iv)** a cascode configuration of a M-BDS and a low-voltage Schottky diode (self-reverse-blocking M-BDS, SRB-M-BDS) [22]; **(c)** SRB-M-BDS-based ac-ac CSC.

Therefore, the full functionality of a dual-gate M-BDS is not strictly needed, but only that of a transistor with a series diode (see **Fig. 11b**). Advantageously, this reduces the number of individual gate control signals and the overall complexity, as the commutation sequences can be simplified (no four-step commutations necessary, see below). However, a dedicated series diode needs to support the full voltage and hence shows high conduction losses. Instead, the advantageous ohmic conduction characteristic of the M-BDS could be retained by controlling one of the M-BDSs two gates *locally* to mimic the diode behavior (synchronous rectification), which requires a gate drive with corresponding sensing capabilities [23]. Alternatively, a cascode arrangement of a M-BDS (featuring one normally-on gate) and a low-voltage Schottky diode can provide the same functionality without sensing electronics, i.e., it achieves a self-reverse-blocking (SRB) behavior and a quasi-ohmic conduction characteristic [22]. The resulting ac-ac CSC VSD topology is shown in **Fig. 11c** and features the same number of gate control signals as its dual, the ac-ac voltage-source converter (VSC) shown in **Fig. 12a**, but again benefits from the lower number of main magnetic components which are advantageously shared between the two converter stages. Note that higher performance (i.e., no conduction loss contribution from a low-voltage Schottky diode, small as it may be) can be achieved by accepting the higher

complexity resulting from directly using dual-gate M-BDSs as shown in **Fig. 12b**. In the future, however, this perceived complexity increase might become irrelevant with further integration of M-BDSs, gate drives, and possibly sensing electronics and commutation logic into intelligent CSR/CSI commutation cell modules.
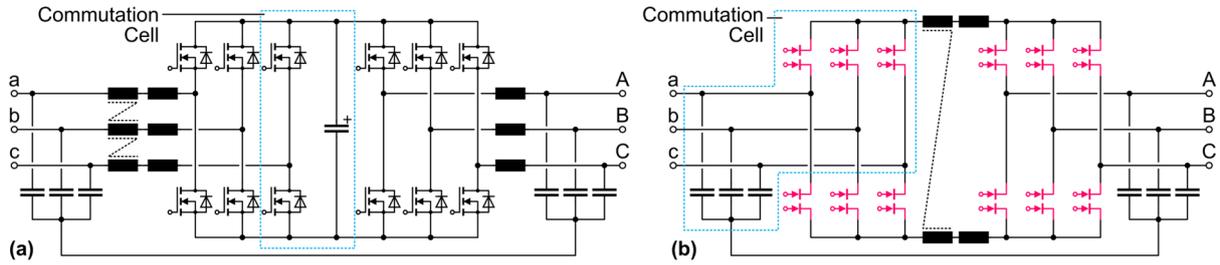

Fig. 12. Core stages of ac-ac VSDs (the full grid-side EMI filters are not shown). **(a)** Voltage-source converter (VSC) with first-stage input and output common-mode (CM) and differential-mode (DM) filters, and boost-buck functionality. **(b)** Current-source converter (CSC) with M-BDSs, integrated first-stage CM and DM filters, and buck-boost functionality. Note that a CSC commutation cell comprises *three* M-BDSs and that the main magnetic components are shared between the converter stages.
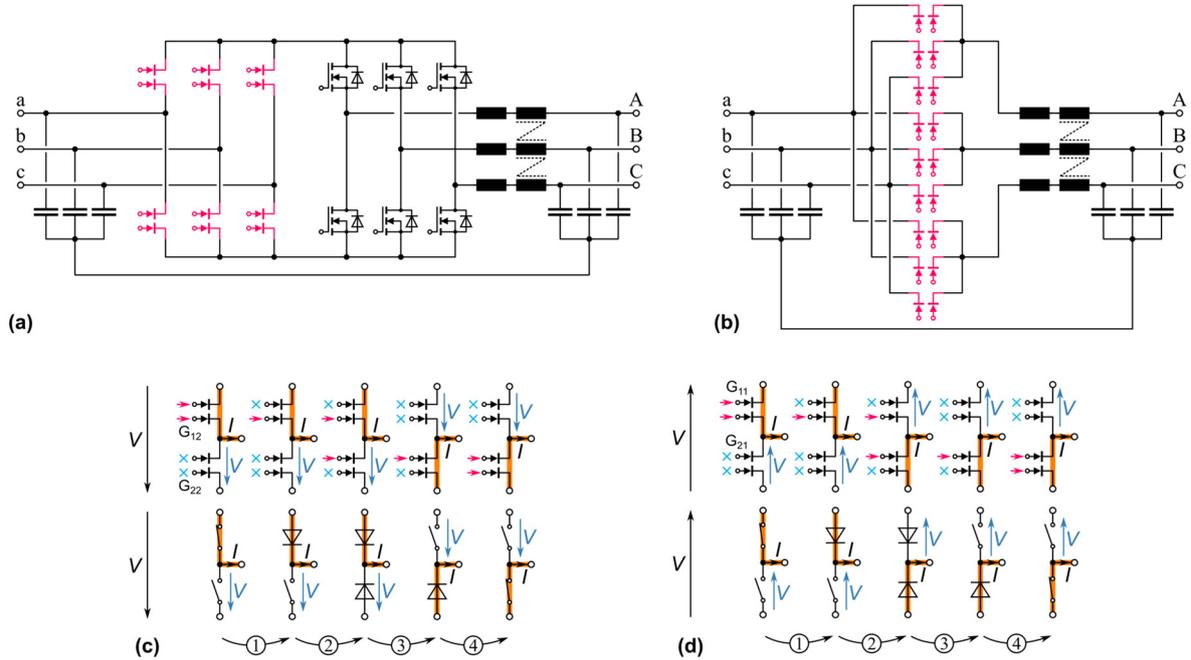

Fig. 13. VSDs based on ac-ac matrix converters. **(a)** Indirect matrix converter (IMC) [24], i.e., a back-to-back configuration of a current-source rectifier (CSR) and a voltage-source inverter (VSI) without intermediate energy storage elements. **(b)** Direct matrix converter (DMC) [2], [3] obtained from merging the IMC's two stages, achieving ac-ac conversion with the minimum of only nine BDSs. **(c)** and **(d)** show current-direction-dependent four-step commutation sequences [25] for DMCs (and also for CSC commutation cells, see **Fig. 12b**) using dual-gate M-BDSs; the second row shows the functional equivalent circuit for each step. Note that safe commutations are achieved regardless of the applied voltage polarity.

As the instantaneous power flow of (symmetric) three-phase systems is constant, it is in principle not necessary to provide an energy buffer (capacitor, inductor) in the dc-link of an ac-ac VSD. Omitting this energy storage element is the key idea of matrix converters such as the indirect matrix converter (IMC) [24] shown in **Fig. 13a**, i.e., a back-to-back arrangement of a CSR and a VSI, featuring a voltage dc-link with strictly positive voltage but without an energy storage capacitor. The two converter stages can be integrated, resulting in the direct matrix converter (DMC) [2], [3] that realizes ac-ac conversion with a minimum of only nine BDSs, see **Fig. 13b**. Both topologies, IMC and DMC, are limited to buck operation; specifically, the maximum motor voltage V_m is limited to $V_m \leq \sqrt{3}/2 \cdot V_g \approx 0.86\,V_g$, where V_g is the grid voltage. Note further that the DMC (and, for that matter, also the commutation cells of CSCs, see **Fig. 12b**) require multi-step commutation sequences to ensure that there is always a path for the inductor current while never short-circuiting any of the capacitors. Typically, four-step commutation sequences that depend on the current direction (see **Fig. 13cd**) [25] or on the voltage polarity [26] are

employed; but also variants with fewer steps have been described. Clearly, the availability of M-BDSs renders the DMC topology a highly attractive realization option for ac-ac VSDs due to the minimal switch count. Thus, for example, a GaN M-BDS-based DMC achieving extreme compactness by massive on-chip/in-PCB integration has been demonstrated in [27], and [28] describes a 2-kW ac-ac DMC operating from a 200 V grid using early discrete dual-gate GaN M-BDSs.

IV. SOLID-STATE CIRCUIT BREAKERS

Finally, M-BDSs might also find use in future ac solid-state circuit breakers (SSCBs) [29]. As **Fig. 14** shows, SSCBs comprise in addition to the power semiconductor itself (which requires BDS capability, at least in ac applications) also an overvoltage protection element, current sensing and control electronics, and possibly an external communication interface that facilitates integration in smart grid environments or advanced remote configuration options such as dynamic adaption of trip levels or utilization as a remote-controlled load switch. Given today's sensing and processing capabilities, SSCBs can react significantly quicker than conventional mechanical circuit breakers, which implies that the switched fault current is limited to relatively low values even if the system's prospective short-circuit current is high. On the other hand, during regular operation the load current flows through the power semiconductors and generates conduction losses. Thus, M-BDSs with an inherently better per-chip-area on-state resistance compared to discrete realizations (see **Fig. 2gh**) are thus attractive for future SSCBs [30]–[32].
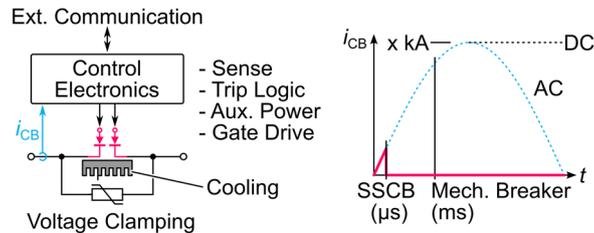

Fig. 14. Key components of an ac solid-state circuit breaker (SSCB) realized with an M-BDS and comparison of the reaction times between an SSCB and a conventional mechanical circuit breaker, see also [29].

V. MONOLITHIC BIDIRECTIONAL SWITCH CONCEPTS

It is beyond the scope of this article to provide a comprehensive history of the M-BDS development. Thus, suffice to say that early activities regarding M-BDS semiconductor realizations can be traced back to the turn of the millennium, where not only reverse-blocking IGBTs (RB-IGBTs) [33] have been demonstrated, but also early M-BDS concepts [34]. A few years later, various companies started to investigate M-BDSs based on GaN HEMTs featuring two individual gates and especially a shared drain region that is used for blocking either voltage polarity [35]–[38]. Thus, GaN M-BDSs can be considered the most mature M-BDS technology, with ±600 V, 140 mΩ samples being available [7], [38]. **Fig. 15a** shows a schematic device cross section of such a normally-off dual-gate GaN M-BDS (gate-injection transistor, GIT); alternative realizations feature normally-on gates or cascode configurations with LV MOSFETs connected in series with either source terminal [39].

SiC-based M-BDSs have been demonstrated recently, too, which would allow for increased blocking voltages above the ±650 V typically achieved with GaN-based lateral device concepts. **Fig. 15b** shows a BiDFET [40], a monolithic (in the sense of on-chip) arrangement of two SiC transistors with integrated JBS diodes. Whereas the BiDFET provides a blocking voltage of ±1200 V, it is essentially a common-drain arrangement of *two* transistors and hence there are *two* drift regions, one for supporting each blocking voltage polarity. Thus, whereas there are benefits from the on-chip inverse-series connection, e.g., regarding handling and packaging, the factor-of-four penalty in chip area usage (see **Fig. 2g**) still applies. The same is true for a vertical back-to-back configuration of two MOSFET dies with a metal interposer layer in-between [41], see **Fig. 15c**. This is in contrast to the true monolithic bidirectional 4H-SiC IGBT device [42] shown in **Fig. 15d**, where the shared drain region is clearly visible; initial prototype devices achieved measured blocking voltages of up to ±7 kV. Such vertical SiC M-BDS concepts, however, require non-standard double-sided lithography processes and are more challenging to cool as both sides of the wafer feature intricate structures (gates, etc.). Finally, **Fig. 15e** shows a recently demonstrated true monolithic bidirectional Si bipolar junction transistor (BJT) with a shared

collector region (B-TRAN™) [43]. The devices achieve a blocking voltage of ±1200 V and support pulsed currents of up to ±100 A, but, being BJTs with a typical current gain of three to four, require relatively complex gate drive circuitry providing the corresponding base currents.
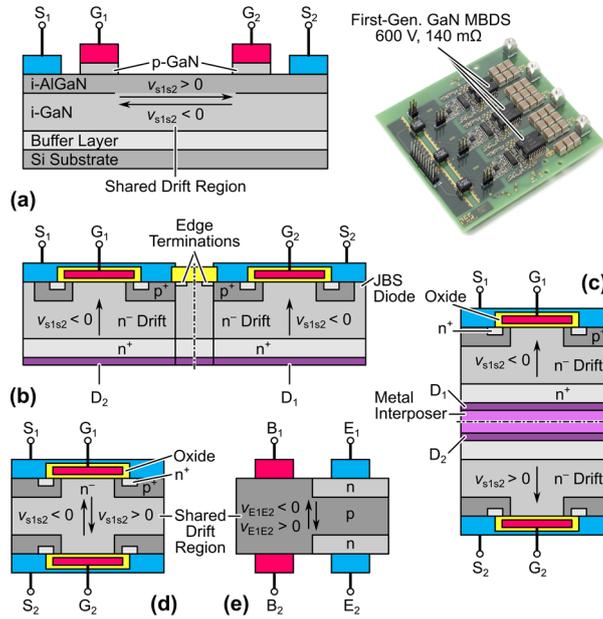

Fig. 15. Conceptual (more details are given in the references) device cross sections of various M-BDSs. **(a)** Monolithic bidirectional dual-gate GaN HEMT [35]–[38] with a single drift region for both blocking voltage polarities, and test board with a CSC commutation cell (see **Fig. 12b**) realized with first-generation ±600 V, 140 mΩ samples [38]. **(b)** SiC BiDFET [40] and **(c)** similar vertical back-to-back connection of *two* SiC MOSFETs [41]. **(d)** Monolithic bidirectional 4H-SiC IGBT with a single drift region [42] and **(e)** B-TRAN™ [43], a monolithic bidirectional Si bipolar junction transistor, also with a single drift region.

VI. CONCLUSIONS

Power electronics is a key enabling technology for solutions to the 21st century's major challenges such as the climate crisis. As outlined in this article, there are many converter topologies (e.g., Vienna rectifiers, current-source or matrix converters, etc.) for key application areas like grid interfaces and motor drives, which require switches with bidirectional voltage blocking and bidirectional current conduction capability, i.e., bidirectional switches (BDSs). These topologies will hence benefit from the availability of dual-gate single-drift-region monolithic bidirectional switches (M-BDSs), which can overcome the factor-of-four penalty in chip area usage of conventional discrete realizations. With M-BDSs removing this structural drawback, these converter topologies become regular members of the family and their suitability for many applications must be reevaluated. In addition, the emergence of M-BDSs inspires the derivation of new topologies, e.g., [44].

GaN M-BDSs are already quite mature and approach commercial availability, but as of now are limited to blocking voltages of up to ±650 V. Whereas this is sufficient for three-level Vienna rectifiers or T-type converters connected to the 400 V mains, it is not for current-source or matrix converters. SiC M-BDSs that would allow higher blocking voltages are considered in research, but the vertical device structures come with challenges such as non-standard two-sided wafer processing and a more complicated interface to cooling systems.

Looking at the technology S-curves of power electronics development cycles shown in **Fig. 16**, it becomes clear that each cycle has been driven by a new power semiconductor technology (see also [45]); most recently by the transition to wide-bandgap (WBG) devices. It can be expected that M-BDSs, especially once higher blocking voltages are achieved either by improved GaN technology (e.g., 1200 V using sapphire substrates [46]) or mature SiC M-BDSs, are, together with superjunction SiC devices [47], and ultra-WBG materials (like diamond) [48], amongst the X-Technologies [49] shaping the ongoing disruptive transition to Power Electronics 4.0. In addition, a further key technology will be the integration (functional and physical) of power switches (e.g., M-BDSs) and surrounding circuitry (gate drives, sensing, commutation logic), aiming at masking complexity (such as four-step commutation sequences) from the application. Also, on the physical level and following trends from microprocessor

technology [50], concepts for monolithic 3D-integration [27] of power, information, and cooling systems will be necessary to achieve highest performance using a minimum of space and resources.
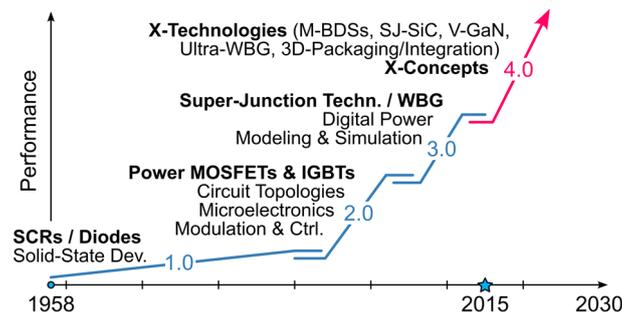

Fig. 16. Technology S-curves of power electronics development cycles, typically triggered by new power semiconductor technologies. Replacement/disruptive technologies improve performance not only by a few percentage points but by factors (i.e., X-Technologies and X-Concepts [49] by a factor *X*).

About the Authors

Jonas Huber (huber@lem.ee.ethz.ch) is a Senior Member of the IEEE and a Senior Researcher at the Power Electronic Systems Laboratory, ETH Zurich, Switzerland. His research interests comprise all types of WBG-semiconductor-based ultra-compact, ultra-efficient or highly dynamic converter systems.

Johann W. Kolar (kolar@lem.ee.ethz.ch) is a Fellow of the IEEE, an International Member of the US National Academy of Engineering and a Full Professor and Head of the Power Electronic Systems Laboratory at the Swiss Federal Institute of Technology (ETH) Zurich. The focus of his current research is on ultra-compact/efficient WBG PFC rectifier and inverter systems, ultra-high bandwidth switch-mode power amplifiers, multi-port converters, Solid-State Transformers, multi-functional actuators, ultra-high speed / motor-integrated drives, bearingless motors, ANN-based multi-objective design optimization, and life cycle analysis of power electronics converter systems.

References

[1] J. W. Kolar and F. C. Zach, "A novel three-phase utility interface minimizing line current harmonics of high-power telecommunications rectifier modules," *IEEE Trans. Ind. Electron.*, vol. 44, no. 4, pp. 456–467, Aug. 1997.

[2] R. F. Blake, W. J. Spaven, and C. C. Ware, "Controlled frequency power supply system," U.S. Patent 3 148 323, Sep. 08, 1964.

[3] L. Huber, D. Borojevic, and N. Burany, "Voltage space vector based PWM control of forced commutated cycloconverters," in *Proc. 15th Annu. Conf. IEEE Ind. Electron. Soc. (IECON)*, Philadelphia, PA, USA, Nov. 1989, pp. 106–111.

[4] M. Jantsch and C. W. G. Verhoeve, "Inverters with three phase output and without electrolyte capacitor for improved lifetime, efficiency and costs of grid connected systems," in *Proc. 14th Europ. Photovoltaic Solar Energy Conf.*, Barcelona, Spain, Jun. 1997, pp. 2198–2200.

[5] J. W. Kolar and T. Friedli, "The essence of three-phase PFC rectifier systems—Part I," *IEEE Trans. Power Electron.*, vol. 28, no. 1, pp. 176–198, Jan. 2013.

[6] J. C. Salmon, "Operating a three-phase diode rectifier with a low-input current distortion using a series-connected dual boost converter," *IEEE Trans. Power Electron.*, vol. 11, no. 4, pp. 592–603, Jul. 1996.

[7] F. Vollmaier, N. Nain, J. Huber, J. W. Kolar, K. K. Leong, and B. Pandya, "Performance evaluation of future T-Type PFC rectifier and inverter systems with monolithic bidirectional 600V GaN switches," in *Proc. IEEE Energy Conv. Congr. Expo. (ECCE USA)*, Vancouver, Canada, Oct. 2021, pp. 5297–5304.

[8] J. W. Kolar, H. Ertl, and F. C. Zach, "Realization considerations for unidirectional three-phase PWM rectifier systems with low effects on the mains," in *Proc. 6th IEEE Int. Power Electron. Motion Control Conf. (PEMC)*, Budapest, Hungary, Oct. 1990.

[9] H. Ueno *et al.*, "A 3-phase T-type 3-level inverter using GaN bidirectional switch with very low on-state resistance," in *Proc. Int. Conf. Power Electron. Intelligent Motion (PCIM Europe)*, Nuremberg, Germany, May 2019.

[10] S. D. Freeland, "Techniques for the practical application of duality to power circuits," *IEEE Trans. Power Electron.*, vol. 7, no. 2, pp. 374–384, Apr. 1992.

[11] J. W. Kolar, H. Ertl, and F. Zach, "Quasi-dual modulation of three-phase PWM converters," *IEEE Trans. Ind. Appl.*, vol. 29, no. 2, pp. 313–319, Mar. 1993.

[12] D. Zhang, M. Guacci, J. W. Kolar, and J. Everts, "Three-phase bidirectional ultra-wide output voltage range current DC-link AC/DC buck-boost converter," in *Proc. 46th Annu. Conf. IEEE Ind. Electron. Soc. (IECON)*, Singapore, Oct. 2020, pp. 4709–4716.

[13] N. D. Weise, K. K. Mohapatra, and N. Mohan, "Universal utility interface for Plug-in Hybrid electric vehicles with vehicle-to-grid functionality," in *Proc. IEEE PES General Meet.*, Minneapolis, MN, USA, Jul. 2010.

[14] L. Schrittwieser, M. Leibl, and J. W. Kolar, "99% efficient isolated three-phase matrix-type DAB buck–boost PFC rectifier," *IEEE Trans. Power Electron.*, vol. 35, no. 1, pp. 138–157, Jan. 2020.

[15] J. W. Kolar, U. Drofenik, and F. C. Zach, "VIENNA rectifier II—A novel single-stage high-frequency isolated three-phase PWM rectifier system," *IEEE Trans. Ind. Electron.*, vol. 46, no. 4, pp. 674–691, Aug. 1999.

[16] K. Vangen, T. Melaa, S. Bergsmark, and R. Nilsen, "Efficient high-frequency soft-switched power converter with signal processor control," in *Proc. 13th Int. Telecommunications Energy Conf. (INTELEC)*, Kyoto, Japan, Nov. 1991, vol. 91, pp. 631–639.

[17] H. Schmidt, C. Siedle, and J. Ketterer, "DC/AC converter to convert direct electric voltage into alternating voltage or into alternating current," U.S. Patent 7 046 534 B2, May 16, 2006.

[18] K. Shirabe *et al.*, "Efficiency comparison between Si-IGBT-based drive and GaN-based drive," *IEEE Trans. Ind. Appl.*, vol. 50, no. 1, pp. 566–572, Jan. 2014.

[19] R. Amorim Torres, H. Dai, W. Lee, B. Sarlioglu, and T. Jahns, "Current-source inverter integrated motor drives using dual-gate four-quadrant wide-bandgap power switches," *IEEE Trans. Ind. Appl.*, vol. 57, no. 5, pp. 5183–5198, Sep. 2021.

[20] M. Guacci, D. Zhang, M. Tatic, D. Bortis, J. W. Kolar, Y. Kinoshita, and H. Ishida, "Three-phase two-third-PWM buck-boost current source inverter system employing dual-gate monolithic bidirectional GaN e-FETs," *CPSS Trans. Power Electron. Appl.*, vol. 4, no. 4, pp. 339–354, Dec. 2019.

[21] T. Friedli, S. D. Round, D. Hassler, and J. W. Kolar, "Design and performance of a 200-kHz All-SiC JFET current DC-link back-to-back converter," *IEEE Trans. Ind. Appl.*, vol. 45, no. 5, pp. 1868–1878, Sep. 2009.

[22] N. Nain, S. Walser, J. Huber, K. K. Leong, and J. W. Kolar, "Self-reverse-blocking control of dual-gate monolithic bidirectional GaN switch with quasi-ohmic on-state characteristic," *IEEE Trans. Power Electron.*, vol. 37, no. 9, pp. 10091–10094, Sep. 2022.

[23] D. Siemaszko and A. C. Rufer, "Active self-switching methods for emerging monolithic bidirectional switches applied to diode-less converters," in *Proc. 13th Europ. Power Electron. Conf. (EPE)*, Barcelona, Spain, Sep. 2009.

[24] K. Shinohara, Y. Minari, T. Irisa, and Y. Imamura, "Analysis and fundamental characteristics of induction motor driven by voltage-source type inverter without DC link components," *Elect. Eng. Jpn.*, vol. 109, no. 6, pp. 56–64, 1989.

[25] N. Burany, "Safe control of four-quadrant switches," in *Conf. Rec. IEEE Ind. Appl. Soc. Annu. Meet.*, San Diego, CA, USA, Oct. 1989, pp. 1190–1194.

[26] J. Oyama, T. Higuchi, E. Yamada, T. Koga, and T. Lipo, "New control strategy for matrix converter," in *Proc. 20th Annu. IEEE Power Electron. Specialists Conf. (PESC)*, Milwaukee, WI, USA, Jun. 1989, pp. 360–367.

[27] S. Nagai, Y. Yamada, N. Negoro, H. Handa, M. Hiraiwa, N. Otsuka, and D. Ueda, "A 3-phase AC–AC matrix converter GaN chipset with drive-by-microwave technology," *IEEE J. Electron Devices Soc.*, vol. 3, no. 1, pp. 7–14, Jan. 2015.

[28] H. Umeda, Y. Yamada, K. Asanuma, F. Kusama, Y. Kinoshita, H. Ueno, H. Ishida, T. Hatsuda, and T. Ueda, "High power 3-phase to 3-phase matrix converter using dual-gate GaN bidirectional switches," in *Proc. IEEE Appl. Power Electron. Conf. Expo. (APEC)*, San Antonio, TX, USA, Mar. 2018, pp. 894–897.

[29] R. Rodrigues, Y. Du, A. Antoniazzi, and P. Cairoli, "A review of solid-state circuit breakers," *IEEE Trans. Power Electron.*, vol. 36, no. 1, pp. 364–377, Jan. 2021.

[30] Z. J. Shen *et al.*, "First experimental demonstration of solid state circuit breaker (SSCB) using 650V GaN-based monolithic bidirectional switch," in *Proc. 28th Int. Symp. Power Semiconductor Devices ICs (ISPSD)*, Prague, Czech Republic, Jun. 2016, pp. 79–82.

[31] Y. Kinoshita, T. Ichiryu, A. Suzuki, and H. Ishida, "100 A solid state circuit breaker using monolithic GaN bidirectional switch with two-step gate-discharging technique," in *Proc. IEEE Appl. Power Electron. Conf. Expo. (APEC)*, New Orleans, LA, USA, Mar. 2020, pp. 652–657.

[32] S. Musumeci, M. Panizza, F. Stella, and F. Perraud, "Monolithic bidirectional switch based on GaN gate injection transistors," in *Proc. 29th IEEE Int. Ind. Electron. Symp. (ISIE)*, Delft, Netherlands, Jun. 2020, pp. 1045–1050.

[33] M. Takei, Y. Harada, and K. Ueno, "600 V-IGBT with reverse blocking capability," in *Proc. 13th Int. Symp. Power Semiconductor Devices ICs (ISPSD)*, Osaka, Japan, Jun. 2001, pp. 413–416.

[34] F. Heinke and R. Sittig, "The monolithic bidirectional switch (MBS)," in *Proc. 12th Int. Symp. Power Semiconductor Devices ICs (ISPSD)*, Toulouse, France, May 2000, pp. 237–240.

[35] D. M. Kinzer and R. Beach, "III-nitride bidirectional switch," U.S. Patent 7 465 997 B2, Dec. 16, 2008.

[36] T. Morita, M. Yanagihara, H. Ishida, M. Hikita, K. Kaibara, H. Matsuo, Y. Uemoto, T. Ueda, T. Tanaka, and D. Ueda, "650V 3.1 mΩcm^2 GaN-based monolithic bidirectional switch using normally-off gate injection transistor," in *Proc. IEEE Int. Electron. Dev. Meet. (IEDM)*, Washington, DC, USA, Dec. 2007, pp. 865–868.

[37] J. Honea, P. Parikh, Y. Wu, and I. Ben-Yaacov, "III-nitride bidirectional switches," U.S. Patent 7 875 907 B2, Jan. 25, 2011.

[38] N. Nain, D. Zhang, J. Huber, J. W. Kolar, K. K. Leong, and B. Pandya, "Synergetic control of three-phase AC-AC current-source converter employing monolithic bidirectional 600 V GaN transistors," in *Proc. 22nd IEEE Control Modeling Power Electron. Workshop (COMPEL)*, Cartagena, Colombia, Nov. 2021.

[39] U. Raheja, G. Gohil, K. Han, S. Acharya, B. Jayant Baliga, S. Battacharya, M. Labreque, P. Smith, and R. Lal, "Applications and characterization of four quadrant GaN switch," in *Proc. IEEE Energy Conv. Congr. Expo. (ECCE USA)*, Cincinnati, OH, USA, Oct. 2017, pp. 1967–1975.

[40] K. Han, A. Agarwal, A. Kanale, B. Jayant Baliga, S. Bhattacharya, T.-H. Cheng, V. Amarasinghe, and J. Ransom, "Monolithic 4-terminal 1.2 kV/20 A 4H-SiC bi-directional field effect transistor (BiDFET) with integrated JBS diodes," in *Proc. 32nd Int. Symp. Power Semiconductor Devices ICs (ISPSD)*, Vienna, Austria, Sep. 2020, pp. 242–245.

[41] C. W. Hitchcock and T. P. Chow, "Common-drain bidirectional 1200V SiC MOSFETs," *Materials Science Forum*, vol. 1004, pp. 882–888, 2020.

[42] S. Chowdhury, C. W. Hitchcock, Z. Stum, R. P. Dahal, I. B. Bhat, and T. P. Chow, "Operating principles, design considerations, and experimental characteristics of high-voltage 4H-SiC bidirectional IGBTs," *IEEE Trans. Electron Devices*, vol. 64, no. 3, pp. 888–896, Mar. 2017.

[43] A. Mojab, J. Bu, J. Knapp, A. Sattar, and D. Brdar, "Operation and characterization of low-loss bidirectional bipolar junction TRANsistor (B-Tran^{TM})," in *Proc. Appl. Power Electron. Conf. Expo. (APEC)*, Houston, TX, USA, Mar. 2022, pp. 205–209.

[44] N. Vosoughi Kurdkandi, O. Husev, O. Matiushkin, D. Vinnikov, Y. P. Siwakoti, and S. S. Lee, "Novel family of flying inductor-based single-stage buck–boost inverters," *IEEE Trans. Emerg. Sel. Topics Power Electron.*, vol. 10, no. 5, pp. 6020–6032, Oct. 2022.

[45] R. V. White, "Which came First? Part I," *IEEE Power Electron. Mag.*, vol. 9, no. 3, pp. 96–94, Sep. 2022.

[46] G. Gupta *et al.*, "1200V GaN switches on sapphire substrate," in *Proc. 34th Int. Symp. Power Semiconductor Devices ICs (ISPSD)*, Vancouver, Canada, May 2022, pp. 349–352.

[47] M. Baba, T. Tawara, T. Morimoto, S. Harada, M. Takei, and H. Kimura, "Ultra-low specific on-resistance achieved in 3.3 kV-class SiC superjunction MOSFET," in *Proc. 33rd Int. Symp. Power Semiconductor Devices ICs (ISPSD)*, Nagoya, Japan, May 2021, pp. 83–86.

[48] H. Umezawa, "Diamond semiconductor devices, state-of-the-art of material growth and device processing," in *Proc. 66th IEEE Int. Electron Dev. Meet. (IEDM)*, San Francisco, CA, USA, Dec. 2020, pp. 5.6.1–5.6.4.

[49] J. W. Kolar and J. Huber, "'X-Concepts' – The DNA of future high-performance power electronic systems," *Keynote presentation at the 1st IEEE Int. Power electron. Appl. Symp. (PEAS),* Shanghai, China, Nov. 2021.

[50] P. Ruch, T. Brunschwiler, W. Escher, S. Paredes, and B. Michel, "Toward five-dimensional scaling: How density improves efficiency in future computers," *IBM J. Res. & Dev.*, vol. 55, no. 5, p. 15:1-15:13, Sep. 2011.